Scanning Electron Microscopy

Volume 1986 | Number 4 Article 6

9-9-1985

Cathodoluminescence Study of Defects in III-V Substrates and Structures

M. Cocito
CSELT

P. Franzosi
MASPEC-CNR

G. Salviati
MASPEC-CNR

F. Taiariol
CSELT

SCANNING ELECTRON MICROSCOPY/1986/IV (Pages 1299-1310)
SEM Inc., AMF O'Hare (Chicago), IL 60666-0507 USA

0586-5581/86$1.00+05

CATHODOLUMINESCENCE STUDY OF DEFECTS IN III-V SUBSTRATES AND STRUCTURES

*M. Cocito(1), P. Franzosi(2), G. Salviati(2), F. Taiariol(1)

(1) CSELT, Torino, Italy (2) MASPEC-CNR, Parma, Italy

(Received for publication January 25, 1984, and in revised form September 09, 1985)

Abstract

Solid state detector cathodoluminescence studies of semiconducting and semi-insulating GaAs and InP crystals, were performed. The origin of the dislocation contrast in GaAs:Si doped substrates, in the carrier concentration range from 10^{16} to $6 \cdot 10^{18}$ cm^{-3}, were discussed. The image contrast was explained on the basis of the emission efficiency versus carrier concentration curve, obtained in the transmission mode. Single dislocations and dislocation arrangements in addition to growth striations, clusters and precipitate-like microdefects were evidenced. The above mentioned microdefects were detected in GaAs:Te, S and Si doped and InP:Sn doped specimens. Commercial InP:Sn and S doped crystals by different manufacturers were also tested in order to perform a comprehensive evaluation of the defect content. Finally, combining emission and transmission cathodoluminescence, Si and Ge detectors at different beam energies, the defect distribution of different layers in simple and double heterostructures was determined in a non-destructive way. MBE InGaAs/InP and LPE InGaAsP/InP structures, employed as semiconductor detectors and lasers, were investigated.

KEY WORDS: Cathodoluminescence, solid state detectors, defects, GaAs, InP, InGaAs, InGaAsP.

*Address for correspondance:
M. Cocito
CSELT, Via R. Romoli, 274
10148 TORINO (Italy)
Phone: 39-11-21691

Introduction

III-V semiconducting materials are assuming increasing importance in both electronic and optoelectronic devices development. GaAs and InP single crystals are used in three different areas of semiconductor technology: i) semi-insulating (SI) crystals with resistivity $\geq 10^7$ $\Omega \cdot cm$ are used as substrates for manufacturing field effect transistors; ii) n-type highly doped ($\sim 10^{18}$ cm^{-3}) substrates are employed to grow epitaxial layers for transferred electron microwave devices; iii) finally, InP and GaAs substrates are necessary for the growth of lattice matched ternary (GaAlAs, InGaAs) and quaternary (InGaAsP, GaAlInAs) epitaxial layers for optoelectronic devices, such as light emitting diodes (LED's), lasers and photodetectors in the 0.9-1.6 μm region.

It is apparent that all the above applications require a good crystal quality in the starting bulk crystals and in the epitaxial layers since yield, reliability and performances of the devices are strongly dependent on the defect content. Therefore, experimental methods able to reveal crystal defects are of great interest.

Among the various techniques, Scanning Electron Microscopy (SEM) cathodoluminescence (CL) is a very powerful one. It is indeed rapid, simple, non destructive and allows one to obtain defect images with quite a good spatial resolution (0.5 - 3 μm). Therefore SEM CL seems to be a good candidate both for routine and basic investigation of crystal perfection in III-V materials.

In this work we shall limit ourselves to GaAs and InP substrates and InGaAs/InP and InGaAsP/InP heterostructures. Moreover, the use of solid state detector cathodoluminescence (SSD-CL) both in the transmission (TCL) and emission (ECL) configurations will be discussed. The aim of this paper is:

1) to confirm the usefulness of the TCL method for substrate defect investigation also in the case of specimens which have a very low doping level (nominally undoped) or SI.

2) to discuss the origin of the dislocation contrast in the cases of GaAs either slightly or heavily doped.

3) to show TCL micrographs, compared, in a few cases, with X-ray topographs and chemical etch pits patterns, obtained for different kinds of defects (dislocations emerging nearly perpendicular to or lying on the surface, dislocation clusters, growh striations and precipitate-like microdefects).
4) to present the main results of a quality control of InP commercially available crystals.
5) to emphasize that by combining ECL, TCL, Si and Ge detectors at different beam energies on the same specimen area, it is possible to determine in a non-destructive way the defect distribution of different layers in complete heterostructures.

Substrate Evaluation

As far as bulk samples are concerned, TCL is normally the best experimental configuration owing to the fact that: i) it presents a higher collection efficiency compared with ECL; ii) it is less sensitive to contamination and surface morphology; iii) it does not restrict the possibility of using other detectors; iv) it allows, in principle, to have information on some kinds of bulk defects.

The experiments were performed on GaAs and InP specimens grown by the Liquid Encapsulated Czochralski (LEC). The GaAs specimens (grown at Maspec Institute), were n-type Si, S and Te doped and SI Cr doped. As to the InP samples, n-type S and Sn doped and SI Fe doped commercial crystals were studied. The crystals were polished to a mirror like finish on the front side and the residual mechanical damage was then removed by a mechano-chemical procedure using a Br_2-CH_3OH (0.5%) solution.

All the TCL observations were carried out at room temperature by using a solid state silicon detector in the experimental arrangement described in detail elsewhere (4,7). In some cases, we performed both X-ray topography (XRT) and chemical etching experiments. As for the XRT, a conventional Lang camera, with a geometrical resolution of a few microns, was employed. Using Cu $K\alpha_1$ radiation, both anomalous transmission (TXRT) and reflection (RXRT) images were taken. As for the defect etching solutions, H_2SO_4:H_2O_2:H_2O (3:1:1) for GaAs and HBr:H_3PO_4 (1:2) for InP were used. Finally, the substrate doping level was determined by a standard Van der Pauw method.

In the following, results of TCL investigation on GaAs and InP bulk samples respectively will be reported and discussed assuming two rather different points of view. In the case of GaAs, it must be underlined that the growth technology is sufficiently established and the crystal quality is rather satisfactory. Therefore, careful experiments for clarifying the dislocation contrast mechanism as a function of doping level and detailed investigation of different kinds of crystal defects could be performed. On the contrary, InP is a less established material as far as crystal perfection is concerned. Therefore, only a survey of commonly exhibited defects and a comparison of commercial crystals by different manufacturers has been undertaken.

GaAs substrates

Emission efficiency versus carrier concentration

To date, due to the decrease of cathodoluminescence emission efficiency with the carrier concentration, those semiconducting samples having a carrier concentration ranging between 10^{17} and 10^{18} cm^{-3} were mainly investigated. On the other hand, since the reliability of the CL technique was recently proved also in the case of Si GaAs crystals (2,8) a study of the emission efficiency as a function of the carrier concentration seems to be necessary in order to clarify the TCL limits. A similar study (3) has been performed using ECL in the case of GaAs:Te doped crystals in a wide doping range ($9 \cdot 10^{16}$ -$4 \cdot 10^{18}$ cm^{-3}) and also in the case of GaAs:Si doped in a more restricted region ($1 \cdot 10^{18}$ -$6 \cdot 10^{18}$ cm^{-3}), by using eight differently doped specimens. The experimental conditions, i.e., accelerating voltage, beam current, magnification, working distance, amplifier gain, beam exposure time and specimen thickness (200 ± 10 μm) were the same for all the crystals. When the TCL intensity was plotted against the carrier concentration, it was possible to sketch a smooth curve through all of the points (see curve A of Fig. 1). TCL intensity reaches a maximum at a doping level of $3 \cdot 10^{18}$ cm^{-3}. At low doping levels, the slope of the curve is not as steep as at high doping levels and the TCL luminescence efficiency is high enough to reveal electrically active defects.

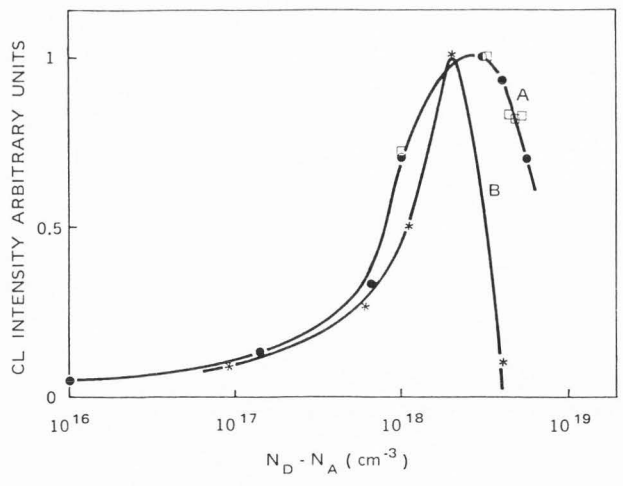

Fig. 1 - Normalized CL intensity curves versus carrier concentration for GaAs:Si (curve A; ● TCL present work, □ ECL reference (3). ECL intensity for GaAs:Te (curve B, reference (3)).

The excellent agreement between the present work and the partial data reported in reference (3), is to be stressed since two different experimental configuration, TCL and ECL respectively, were used. Fig. 1 also shows the ECL curve (B) concerning GaAs:Te doped crystals (3). Comparing in more detail the two curves, the following can be noted: i) on the low doping side the curve coincides as expected; ii) the maximum of curve A is shifted towards higher doping levels, due to the higher Si precipitation threshold: iii) the top of curve A is flatter than that of curve B.

The above mentioned features will be employed in the next section in discussing the dislocation contrast.

Dislocation contrast

On the basis of these results and following a former interpretative scheme (1, 9, 11) we have studied the different contrast exhibited by dislocations in samples with different doping concentrations. As far as the typical dislocation contrast is concerned, it is well known that this kind of defect behaves as a non-radiative recombination centre and for this reason it produces a black spot in CL micrographs. Analyzing specimens with different doping levels, it was possible to establish that sometimes the dislocation contrast is more complex than the simple black spot, due to the impurities gettering by dislocations. Three GaAs:Si differently doped specimens (10^{16}, $3\cdot10^{18}$, $6\cdot10^{18}$ cm^{-3}), which correspond respectively to the left side, the maximum and the right side of curve A in Fig. 1, were investigated together with a GaAs:Te ($1\cdot4\cdot10^{18}$ cm^{-3}) doped sample corresponding about to the maximum of curve B in Fig. 1.

Fig. 2a shows dislocations which emerge at right angles on the specimen surface and some others which are inclined in a GaAs:Si doped (10^{16} cm^{-3}) specimen. The dislocation image consists of a black spot surrounded by a white halo. This contrast can be explained by assuming an increase in the carrier concentration around the dislocation, due to the impurity gettering effect without any doping precipitation on the dislocation itself. In fact, from curve A of Fig. 1 it can be noted that a doping level increase corresponds to a luminescence efficiency increase (white halo). When the GaAs:Si doped ($3\cdot10^{18}$ cm^{-3}) specimen of Fig. 2b is considered, in addition to some growth striations, the micrograph shows dislocation emerging at approximately right angles with respect to the surface. The dislocation image exhibits the typical black dot contrast, but lacks the white halo. Supposing that the dislocations are decorated, a doping reduction around the dislocation and an increase on the defect core are to be considered. Since this specimen has an average doping concentration corresponding to the maximum of curve A of Fig.1 and since the top of the curve is relatively flat, a doping decrease around the dislocation does not cause any significant contrast. In Fig. 2c a TCL micrograph of a GaAs:Si doped ($6\cdot10^{18}$ cm^{-3}) specimen is shown. In addition to a fine structure due to microdefects (probably Si precipitates), the TCL micrographs shows a few dislocations whose black spot is surrounded by a white halo. Due to the very low CL emission efficiency the contrast of this micrograph is weak and both the microdefects and the halo are rarely visible. Also in this case, the contrast can be interpreted by supposing that dislocations, surrounded by a depletion zone, are decorated. From curve A of Fig. 1, it can be observed that on the high dopant side a doping decrease causes an emission increase (white halo).

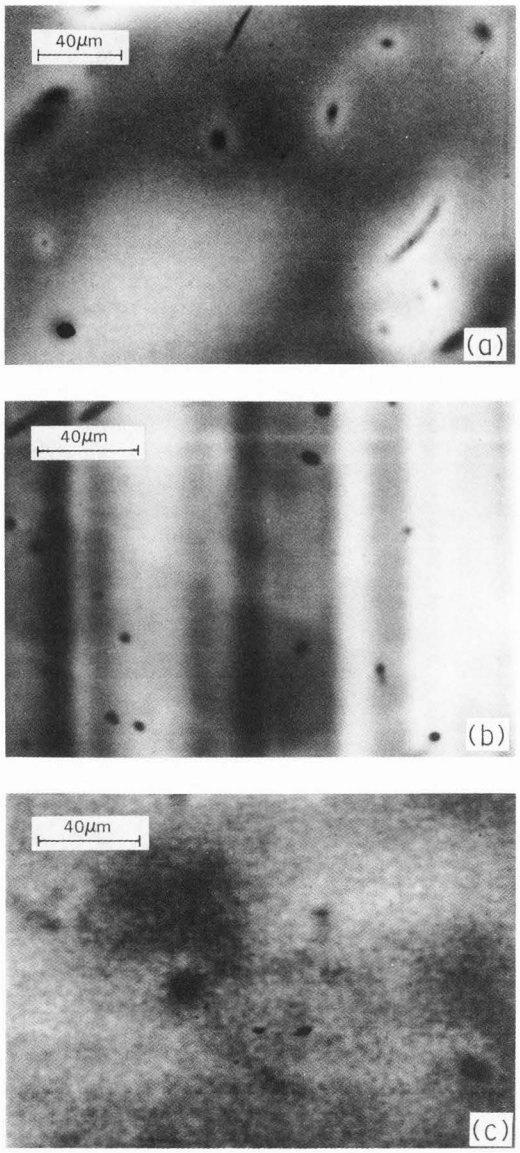

Fig. 2 - Dislocations in differently doped GaAs:Si substrates: a) TCL-Si micropgraph of $1\cdot10^{16}$ cm^{-3} (100) oriented crystal; b) TCL-Si micrograph of $3\cdot10^{18}$ cm^{-3} (111) oriented crystal; c) TCL-Si micrograph of $6\cdot10^{18}$ cm^{-3} (111) oriented crystal.

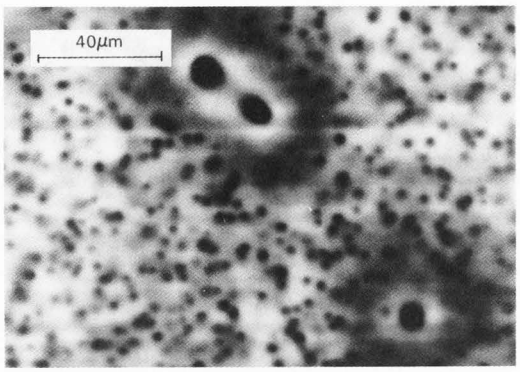

Fig. 3 - Dislocations and precipitate in GaAs:Te (1.4 10^{18} cm^{-3}) substrates. TCL-Si.

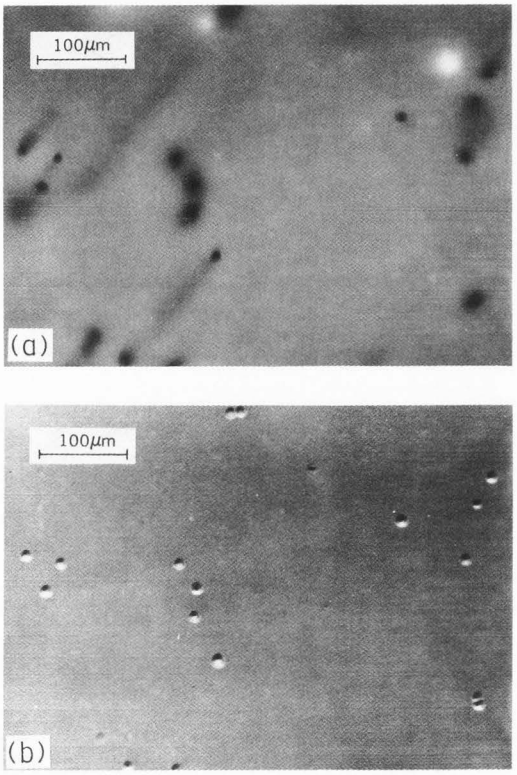

Fig. 4 - Dislocations in SI GaAs:Cr substrate: a) TCL-Si micrograph; b) secondary electron image of the same area after chemical etching.

Fig. 3 shows a GaAs:Te doped ($1{\cdot}4{\cdot}10^{18}$ cm^{-3}) specimen. In addition to a fine structure of small dark spots, a few dislocations (larger dark spots) are present. The dislocation image consists of an external dark grey halo, an intermediate pale grey zone, having the same intensity as the background) and a central black dot. Once again, the dislocation induces a surrounding depletion zone as well as a decoration (1,11). The average doping level corresponds to approximately the top of curve B in Fig. 1 where the maximum is rather narrow. Therefore, the doping decrease in the depletion zone induces a signal decrease (dark grey halo), while the subsequent doping increase towards the average level causes an increase in the emission signal (pale grey zone). Finally, the dislocation decoration combined with the non-radiative recombination effect gives rise to the black central core.

In addition to semiconducting single crystals, GaAs:Cr doped SI specimens were analyzed. A typical TCL micrograph is shown in Fig. 4a and is compared with the etching image on the same crystal region in Fig. 4b. A one-to-one correspondence between etch pits and dislocations is well evidenced. The dislocation TCL image consists of a black dot without any white halo. This could probably be due to the different role that the Cr has with respect to an active dopant in a highly doped GaAs.

Growth striations

Figs. 5a and 5b show TCL and TXRT images of similar areas of GaAs:Si doped ($3{\cdot}10^{18}$ cm^{-3}) (110) oriented specimen cut parallel to the (111) pulling direction. TCL and TXRT images have a comparable spatial resolution even if the origin of the contrast mechanism is completely different (periodic doping variation in the former and periodic variation with consequent anisotropic stress in the latter case). A more detailed discussion on these features is reported in previous papers (6,7).

The shape of the growth striations is related to the evolution of the solid-liquid interface during the crystal growth. For instance, the straight striations of Fig. 5, that were seen at the centre of the ingot, confirm the formation of single facets on the (111) planes. Growth striations are also shown in Fig. 6a, that presents a TCL micrographs of a GaAs:Si doped ($2{\cdot}10^{17}$ cm^{-3}) (100) oriented specimen. The growth striations now are nearly circular with a weak and blended contrast and they show that during the crystal growth a periodical modulation of the doping content took place. Fig. 6b shows a TXRT image of the same area. The picture does not evidence any striation, probably because the lattice parameter variation is below the sensitivity of our technique ($\Delta a/a \sim 10^{-3}$).

Finally, in Fig. 7 TCL micrograph of a GaAs:Te doped ($1.4{\cdot}10^{18}$ cm^{-3}) (111) oriented specimen is shown. Besides a high dislocation density (evidence of the low efficiency of Te for limiting the number of dislocations) growth striations are clearly shown. The striation aspect is different from that of the Si doped specimens. In the latter case, the bands do not have any internal structure and are spotless, thus evidencing that the only difference is their different doping level. In the Te doped specimen, on the contrary, the bands are due to different microdefect concentrations.

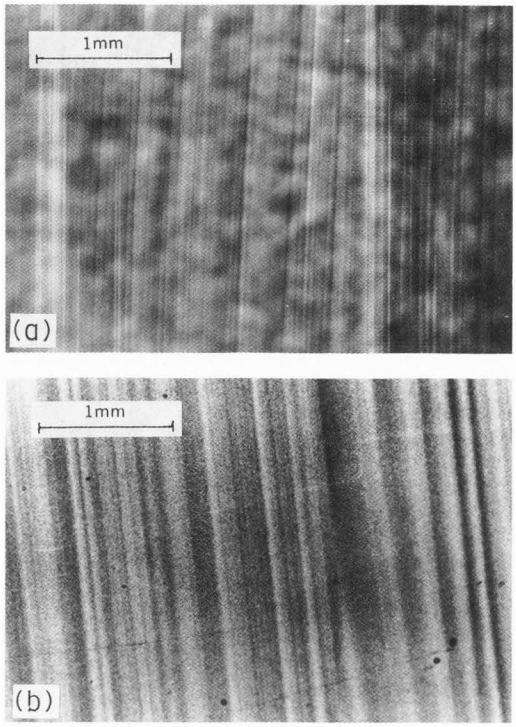

Fig. 5 - Growth striations in GaAs:Si ($3 \cdot 10^{18}$ cm^{-3}) (110) oriented substrate: a) TCL-Si micrograph; b) TXRT image of a similar area.

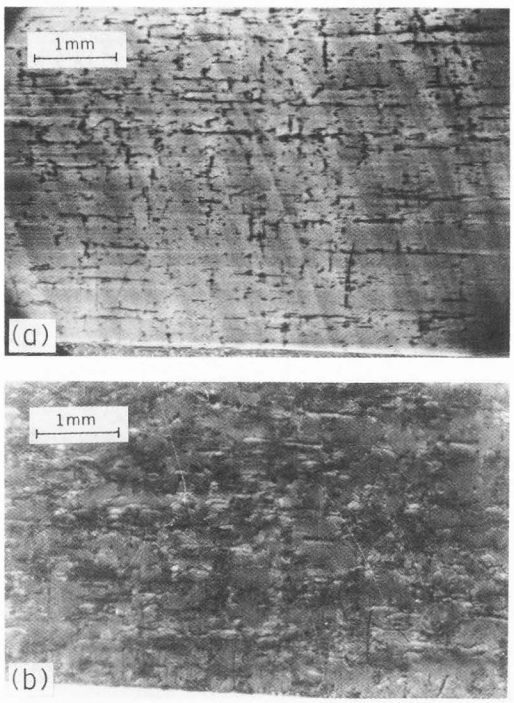

Fig. 6 - Dislocations and growth striations in GaAs:Si ($2 \cdot 10^{17}$ cm^{-3}) (100) oriented substrate: a) TCL-Si micrograph; b) TXRT image of the same area.

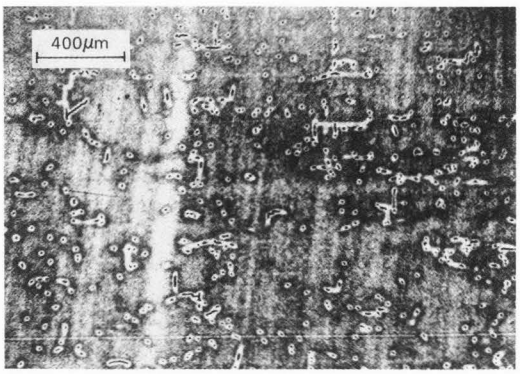

Fig. 7 - Dislocations and growth striations in GaAs:Te ($1.4\ 10^{18}$ cm^{-3}) (111) oriented substrate. TCL-Si.

Precipitate-like microdefects

As briefly mentioned in the above sections, high microdefect densities were observed in GaAs: Te, S and Si doped specimens. In the first case (Fig. 3), the contrast associated with the microdefect should be made up of a dark spot surrounded by a lighter halo. This halo is not visible because of the high defectual density and because of the consequent overlapping of the images. As already mentioned, the most probable hypothesis is that Te precipitates are present. An analogous situation was observed for the first time in GaAs:Si doped (111) oriented specimens as already shown in Fig. 2c. In both cases, due to high impurity concentration, the dislocation density is lower than the microdefect one (ranging from $5 \cdot 10^5$ to 10^6 cm^{-2}). In addition to this, the microdefect dimensions (~ 1-3 μm) are much smaller than those of dislocations.

Fig. 8 shows a TCL picture of a GaAs:S ($3 \cdot 10^{18}$ cm^{-3}) (111) oriented specimen. Microdefects generally present a white contrast with, in some cases, a dark spot in the middle of the white area. Due to the high signal level, the

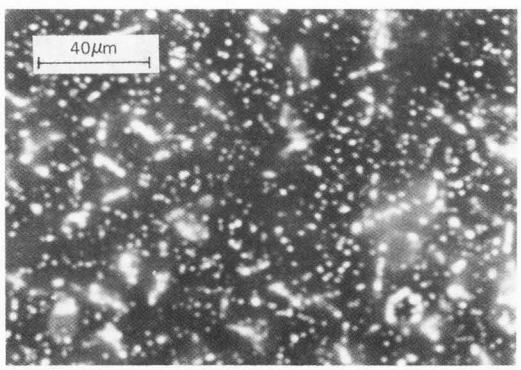

Fig. 8 - Microdefects in GaAs:S ($3 \cdot 10^{18}$ cm^{-3}) (111) oriented substrate. TCL-Si.

brightness of the white area is so strong that it dominates the picture. Further investigations are required to clarify this contrast and the nature of the microdefects; also in this case we have tentatively interpreted these microdefects as being precipitates.
It must be noted that in all the cases involving microdefects, which have been mentioned up to now, investigations by the X-ray double crystal technique tend to support the interpretation involving precipitates. Finally, it must be stressed that the above results indicate that in the case of Te doping the critical threshold for microdefects precipitation is about $1 \cdot 10^{18}$ cm^{-3}, while for Si doping it is about $6 \cdot 10^{18}$ cm^{-3} and for S doping is about $3 \cdot 10^{18}$ cm^{-3}. These last two data were never reported in the literature, probably due to the very high dopant concentration.

InP substrates

Survey on typical defects

TCL investigations of InP bulk samples evidenced a variety of crystal defects similar to those observed in GaAs samples. Dislocations, growth striations, precipitates and clusters of dislocation loops were all observed. For example, Fig. 9 reports a TCL micrograph of a Sn doped ($2 \cdot 10^{18}$ cm^{-3}) (100) oriented sample, where growth striations and dislocations are clearly shown together with some scratches (indicative of the difficulties inherent in polishing and handling InP crystals). A closer inspection of Fig. 9 also reveals the presence of a very high density of microdefects, thickened along striations. Therefore, the hypothesis of Sn precipitates can be reasonable.

Fig. 10 shows a TCL image of an InP:Sn doped ($3.8 \cdot 10^{18}$ cm^{-3}) (100) oriented sample, where dislocations lying parallel to the surface plane are seen as narrow lines mainly oriented along (110) directions. This result was confirmed by TXRT images. A detailed analysis of the Burgers vectors showed that the dislocations are of screw type.

Two extended defects typical of InP crystals are shown in Fig. 11a, where cross-shaped defects and four dot arrangements are shown. It can be noted that the arms of the cross-shaped defects are lying along (110) directions, while the diagonals of the four dot arrangements are parallel to the (100) directions. Comparing the TCL image of Fig. 11a with the RXRT picture of the same crystal region shown in Fig. 11b, a close correspondence between the above defects and the white features exhibited by the RXRT image is confirmed. Features similar to those shown in Fig. 11b are reported in the literature (12) and intrepreted as being due to an unusual inclusion-like defect consisting of a central core from which prismatic dislocation loops are punched out in the (110) directions. On the basis of this model, it can be assumed that the two different defect shapes observed by TCL correspond to similar defects localized at different depths with respect to the sample surface.

The TCL micrograph reported in Fig. 12 shows that the arms of the cross-shaped defect are really composed of dislocation loops and evidences a better spatial resolution of TCL in comparison with the XRT one. However, if on one hand it is possible to distinguish the single loops, on the other hand it is not possible to pick out the core of the defect. It must be noted that the projection of the loop onto a perpendicular plane gives an image less than 2 μm while the defect core is about 5-10 μm. Even if the experimental conditions were varied, it was not possible to improve the image resolution.

Finally, in Fig. 13a TCL image of a SI InP:Fe doped (100) oriented crystal is shown and compared with an etching picture of the same area. A good correspondence between dislocations and etch pits can be observed (13b). Once again, the reliability of the TCL technique for imaging crystal defects at room temperature in SI specimens is confirmed. However, owing to the lack of information on the emission efficiency versus carrier concentration for InP:S and Sn crystals, no discussion on the TCL image contrast can be made.

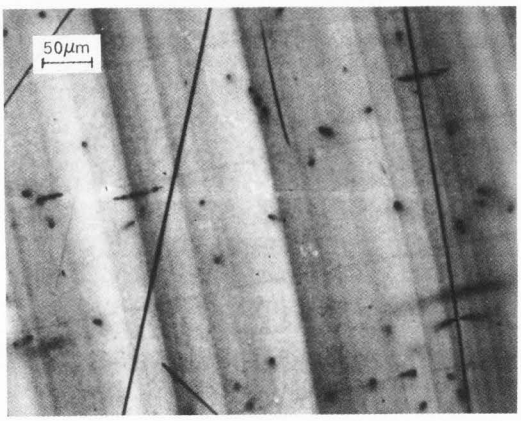

Fig. 9 - Dislocations, growth striations, scratches and microdefects in InP:S ($2 \cdot 10^{18}$ cm^{-3}) (100) oriented substrate. TCL-Si.

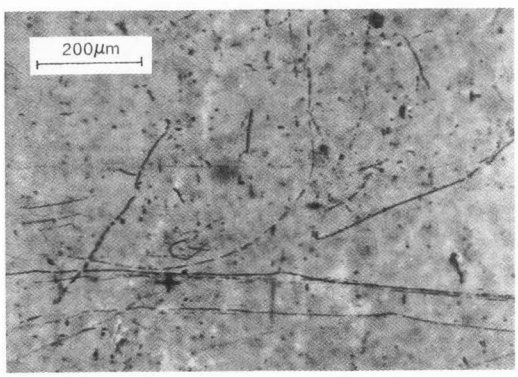

Fig. 10 - Dislocations in InP:Sn ($3.8 \cdot 10^{18}$ cm^{-3}) (100) oriented substrate. TCL-Si

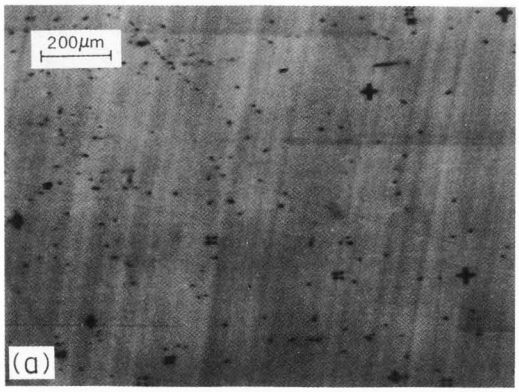

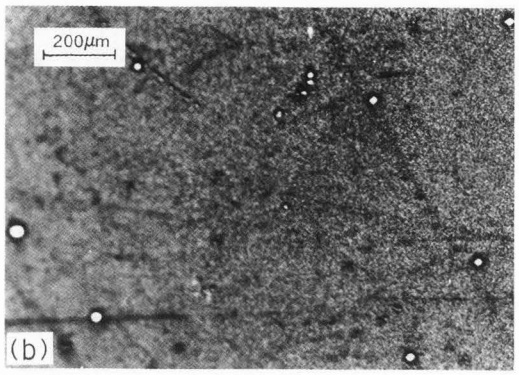

Fig. 11 - Extended defects InP:Sn (3.8 10^{18} cm^{-3}) (100) oriented substrate. a) TCL-Si micrograph; b) RXRT image of the same area.

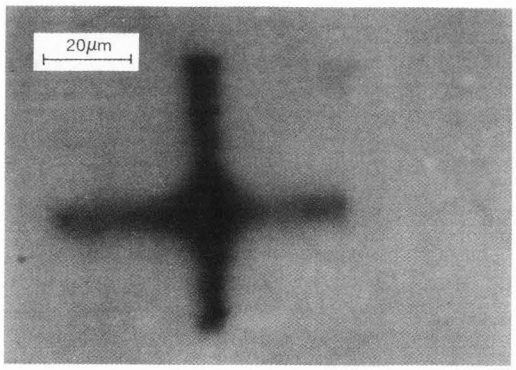

Fig. 12 - Cluster of dislocation loops in InP:Sn ($3.8 \cdot 10^{18}$ cm^{-3}) (100) oriented substrate. TCL-Si.

Commercial substrate quality

Since TCL is a simple, rapid and non-destructive technique, its use for routine quality control was recently proposed (4). We have indeed performed a comprehensive investigation of the defect content in commercially

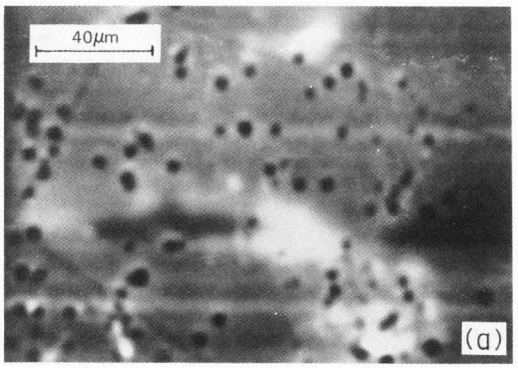

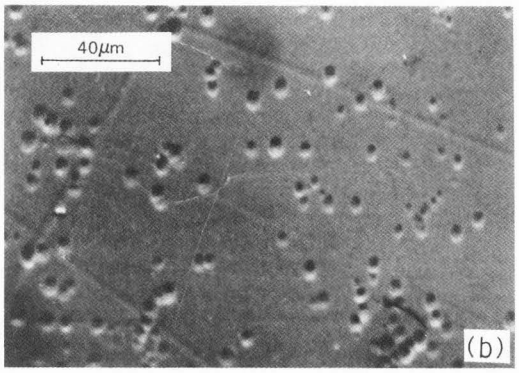

Fig. 13 - Dislocations in Si InP:Fe (100) oriented substrate: a) TCL-Si micrograph; b) secondary electron image of the same area after chemical etching.

available and nominally similar InP crystals produced by different manufacturers. Sn doped crystals from five different sources and S doped crystals from four sources were considered. In both cases the doping level is similar (from $1.2 \cdot 10^{18}$ to $3.8 \cdot 10^{18}$ cm^{-3} for Sn doping, from $6 \cdot 10^{17}$ to $8 \cdot 10^{18}$ cm^{-3} for S doping). The declared etch pit density is about 10^3 cm^{-2} in Sn doped crystals.

The imaged defects are mainly of two types: i) residual damage and damage induced defects; ii) native crystal defects. In the latter case, single dislocations, dopant striations and clusters of dislocation loops were all revealed and quantitatively evaluated. In one case, unidentified defects, whose TCL shape is neither simple as for single dislocations nor clearly distinguishable as for the clusters described in the above section, was observed (Fig. 14).

Tables 1 and 2 summarize the results on defect type and density for the various InP substrates. The tables are self-explanatory and evidence the potentiality of the TCL technique in performing routine quality investigations on commercial crystals. This quality control is of great importance in view of subsequent technological processes, as a high crystal quality is a prerequisite for obtaining high yield and high reliability devices.

Tables 1 and 2: Summary of the results on defect type and density for the verious InP substrates.

DEFECTS	InP (100) SUBSTRATES				
	MCP Sn: 1.2×10^{18} cm^{-3} epd 2.3×10^{4} cm^{-2}	SUMITOMO Sn: 1.9×10^{18} cm^{-3} epd $<10^{4}$cm^{-2}	ORIENTAL SC. INSTR Sn: 2×10^{18} cm^{-3} epd $<4\times10^{4}$ cm^{-2}	CRYSTA COMM INC. Sn: 3.8×10^{18} cm^{-3} epd 3.7×10^{4} cm^{-2}	LASERTRON Sn: 1.5×10^{18}cm^{-3} epd $<3\times10^{4}$ cm^{-2}
SINGLE DISLOCATIONS (cm^{-2})	2.1×10^{4}	3×10^{4}	2×10^{4}	4.8×10^{4}	1.8×10^{5}
DISLOCATION CLUSTER (cm^{-2})	VERY FEW	NO	NO	1.6×10^{3}	NO
RESIDUAL DAMAGE	NO	VERY WEAK	STRONG	NO	VERY STRONG
INDUCED DISLOCATIONS	NO	NO	NO	NO	YES
DOPANT STRIATIONS	YES	YES	YES	YES	NO

Table 1

DEFECTS	InP (100) SUBSTRATES			
	MCP S: 6×10^{17} cm^{-3} epd 5×10^{3} cm^{-2}	SUMITOMO S: 8×10^{18} cm^{-3} epd 10^{2}	ORIENTAL SC. INSTR. S: 3.3×10^{18} cm^{-3} epd 3×10^{3} cm^{-2}	CRYSTA COMM INC. S: 5×10^{18} cm^{-3} epd 1×10^{3} cm^{-2}
SINGLE DISLOCATIONS (cm^{-2})	2.8×10^{3}	2.4×10^{3}	1.2×10^{4}	?
DISLOCATION CLUSTER (cm^{-2})	NO	NO	NO	NO
RESIDUAL DAMAGE	NO	NO	WEAK	VERY WEAK
INDUCED DISLOCATIONS	NO	NO	NO	NO
DOPANT STRIATIONS	YES	YES	YES	NO
UN IDENTIFIED DEFECTS	NO	NO	NO	1.4×10^{6}

Table 2

Structure Evaluation

Liquid Phase Epitaxy (LPE) InGaAs/InP double heterostructure (DH's) and Molecular Beam Epitaxy (MBE) InGaAs/InP single heterostructures are very interesting for realizing respectively light emitters and detectors for optical fiber communications in the 1.3 or 1.6 μm wavelength region. As far as the structure perfection is concerned, it must be stressed that in addition to crystal defects (dislocations, clusters, stacking faults, precipitates), surface morphological imperfections (hillocks, holes, inclusions, voids) of the different layers or interfaces can affect the performances of optoelectronic devices (LED's, lasers, detectors).

CL technique is well suited to study both kinds of defects (5). As epitaxial structures contain different energy gap materials, two phenomena must be considered: i) the generated CL is composed of different wavelength radiations; ii) the various wavelengths can be differently absorbed inside the specimen. These two features when well managed, represent new contrast mechanism which can provide useful information. In fact, combining observations by ECL and TCL and using Si and Ge derectors at various beam energies on the same specimen area, it is possible to deduce, in a non-destructive way, the nature and location of defects. Under proper experimental conditions, the most significant contribution to the signal comes only from one layer. Since each layer has its own set of optimum experimental conditions, a series of CL images, each corresponding to a different layer, can be obtained. Therefore, it is possible to resolve the various layers of a complete structure. This sort of "depth resolution" makes CL a very interesting technique for perfection studies of heterostructures.

InGaAs/InP LPE structures

The first step of any LPE growth is the substrate heating. For InP substrates this step produces a localized P evaporation, the formation of In rich melt droplets and the development of surface pits. These thermal etch pits are usually removed in the second growth step, the pure In melt back etch. However, if the surface pits are not completely removed, they can negatively affect the morphological quality of the epitaxial layers and/or interfaces. Otherwise, a non-satisfactory morphology influences both device yield and reliability. It has indeed been reported that layer thickness variations, inclusions or voids are detrimental to device fabrication (10) and can activate dark line defects (DLD's) during the device life (13).

Fig. 15 refers to an LPE InGaAsP/InP DH sample (with the active layer emitting at 1.2 μm) and shows the non-destructive detection of substrate thermal etch pits not completely removed and filled up by the InP buffer layer. Since the more doped buffer layer exhibits a higher luminescence efficiency that the substrate (Sn doped $3\cdot10^{18}$ and $1\cdot10^{18}$ cm^{-3} respectively), thermal etch pits are observed as comet-like white segments. It must be underlined that the substrate-buffer layer interface was 4 μm under the quaternary layer surface.

If the InP substrate contains dislocation clusters, the pure In melt back etch does not produce a flat surface, but develops hillocks (25 to 30 μm in diameter, a few microns thick) (5). Once again, the subsequent epitaxial growth is strongly influenced. The layer thickness is indeed non uniform and the crystal quality is poor where hillocks are present. The deleterious effects on the devices, are similar to those described for residual thermal etch pits.

Fig. 16a shows a secondary electron image of a hillock covered by a 0.5 μm thick not intentionally doped LPE InGaAsP layer grown on InP:Sn ($1\cdot10^{18}$ cm^{-3}) substrate. In the TCL-Ge image of the same area (Fig. 16b), the main contribution to the signal comes from the quaternary layer. The micrograph shows a non homogeneus layer thickness surrounding the hillock (brighter areas corresponding to larger thickness). In addition to this, black spots related to small morphological defects and dark lines are evidenced on the epilayer. The central dark area is a dislocation cluster in the substrate probably propagating in the epilayer. The TCL-Si image at higher energy (Fig. 16c) shows a reverse contrast in the hillock region since the only contribution is due

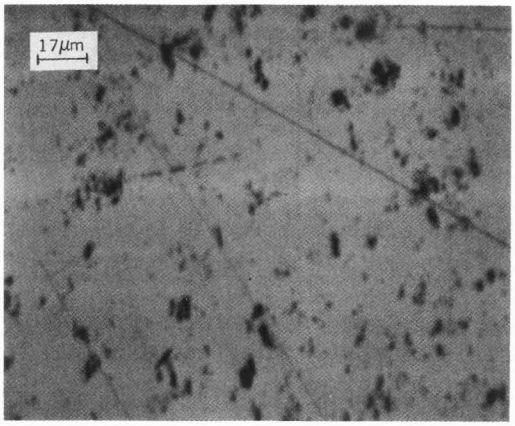

Fig. 14 - Unidentified defects in InP:S ($5 \cdot 10^{18}$ cm^{-3}) (100) oriented substrate. TCL-Si.

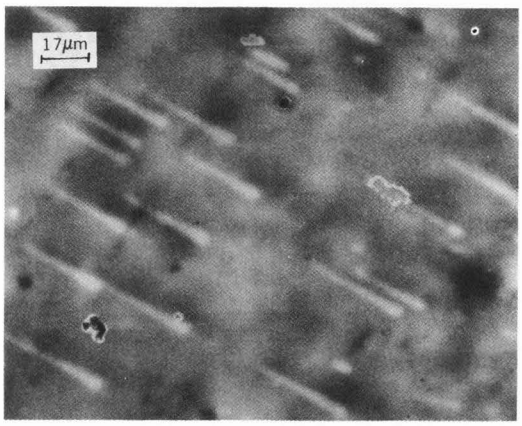

Fig. 15 - Residual thermal etch pits at the substrate-buffer layer interface of an LPE InGaAsP/InP double heterostructure TCL-Si 35 keV.

to the substrate. The appearance of typical substrate defects, showing the usual contrast, at the upper left corner of the micrograph confirms this statement. This analysis repeated on many hillocks showed that under each hillock a dislocation cluster was present. Using cluster free substrates the hillocks disappeared.

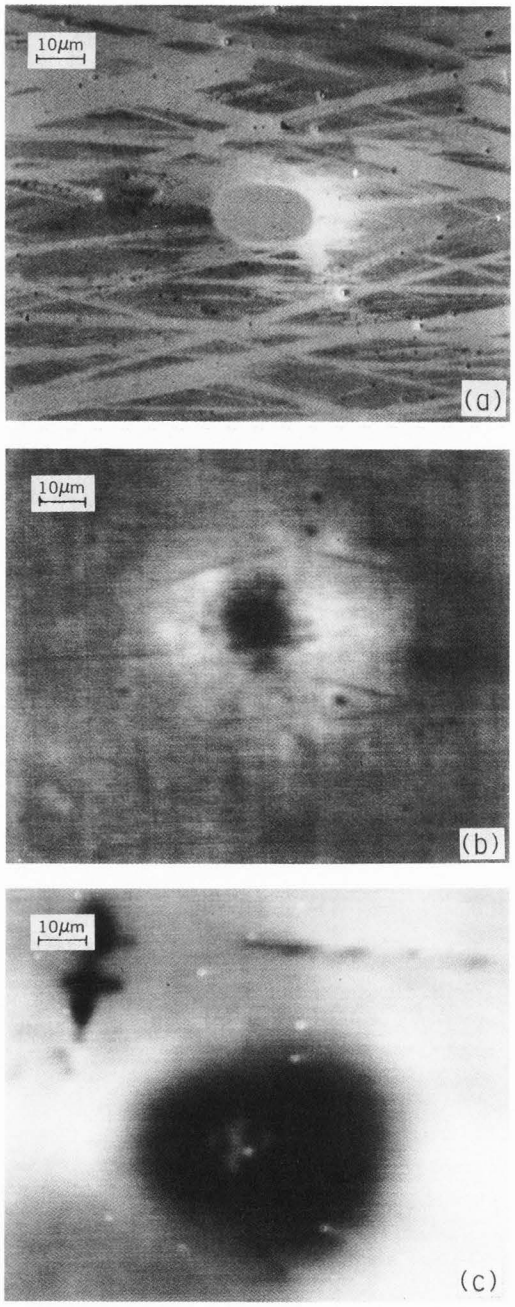

Fig. 16 - Hillock on an LPE InGaAsP/InP single heterostructure: a) secondary electron image; b) TCL-Ge image, 25 keV; c) TCL-Si image, 35 keV.

InGaAs/InP MBE structures

The growth of high yield InGaAs/InP MBE structures for detectors is prevented by the occurrence in the epitaxial layer of a high density of morphological defects which behave as recombination regions. TCL analysis demonstrates that these defects originate mainly from the substrate-layer interface without any correlation with the substrate crystal defects.

Fig. 17a shows a backscattered electron image of a 1.7 μm thick Si doped ($3 \cdot 10^{17}$ cm^{-3}) MBE InGaAs layer emitting at 1.7 μm grown on InP:Sn ($1 \cdot 10^{17}$ cm^{-3}) substrate. The micropgraph shows that the layer contains a high density of morphological defects (10^5 cm^{-2}). Fig. 17b reports a TCL-Ge image at low beam energy where the carrier recombination at the epilayer defects

is evidenced. Finally, Fig. 17c shows a TCL-Si image at higher beam energy and displays the crystal defects of the underlying substrate. No correlation emerges between the defect patterns of layer and substrate. Therefore the defect origin has been traced to anomalous nucleation points caused by contamination residues on the substrate. Improving the substrate cleaning procedures a defect reduction of three orders of magnitude (to about $5 \cdot 10^2$ cm^{-3}) was achieved.

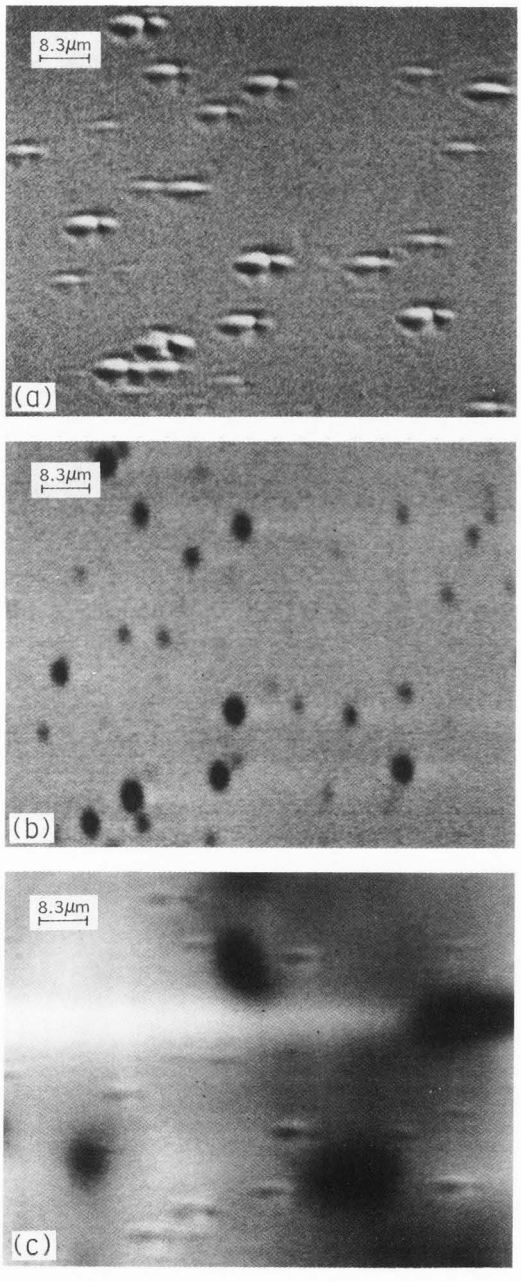

Fig. 17 - Morphological and crystal defects of an MBE InGaAs/InP single heterostructure: a) backscattered electron image; b) TCL-Ge image, 15 keV; c) TCL-Si image, 45 keV.

Conclusions

In this paper we have shown that SSD-CL is a powerful tool for investigating native and process induced defects in III-V compounds substrates and structures. As far as substrates are concerned this technique has been usefully employed both for basic and routine investigations on crystal perfection. A variety of different crystal defects has been evidenced in variously doped specimens. Precipitate-like microdefects have been observed for the first time by TCL in S and Si doped GaAs crystals. The TCL emission efficiency versus carrier concentration curve in a wide doping range for GaAs:Si doped crystals has also been obtained. On the basis of this curve, the dislocation image contrast has been qualitatively explained. A comprehensive defect investigation of InP commercial crystals has shown the TCL suitability for routine quality control.

The combination of TCL, ECL, Si and Ge detectors at various beam energies, allowed a nondestructive evaluation of different layers inside epitaxial heterostucture. In this respect the main results achieved were: i) detecting the residual thermal etching at the substrate-first layer interface and the residual hillocks due to dislocation clusters in an InGaAsP/InP LPE DH; ii) showing that morphological defects from the substrate-layer interface in a InGaAs/InP MBE structure, do not have any correlation with the substrate crystal defects.

The usefulness of complementary techniques, such as XRT and chemical etching, has also been stressed. In addition to this, spectral emission studies at different temperatures could be employed for clarifying some contrast mechanisms, while transmission electron microscopy could permit a sure identification of some microdefects.

Acknowledgements

The authors would like to thank Dr. L. Zanotti and coworkers for the GaAs crystals, Dr. C. Papuzza for the LPE structures, Dr. F. Genova for the MBE structures, Mr. F. Gorgellino and Mr. M. Scaffardi for technical assistance.

References

[1] Balk L.J., Kubalek E., Menzel E., (1976). Investigation of as-grown dislocations in GaAs single crystals in the SEM. Scanning Electron Microsc. 1976; I: 257-264.

[2] Chin A.K., Von Neida A.R., Caruso R. (1982) Investigation of crystal defects in GaAs by X-ray topography and SEM transmission cathodoluminescence. Materials Chemistry and Physics 9, 321-328

[3] Chu Y.M., Darby D.B., Booker G.R., (1981) SEM CL and TEM studies of Te and Si-doped GaAs. Proceedings of 2nd Oxford Conference on: Microscopy of Semiconducting Materials. The Institute of Physics Conference Series N. 60; 331-338.

[4] Cocito M., Gorgellino F., Troia A. (1982) SEM transmission cathodoluminescence: detection system and applications to defects evaluation in III-V compound semiconductors. Proceedings of 10th International Congress on Electron Mcroscopy. Hamburg 2, Deutsche Gesellschaft für Elektronenmikroscopie e.V. 417-418

[5] Cocito M., Papuzza C., Taiariol F. (1983) Emission and transmission cathodoluminescence analysis of InGaAsP/InP LPE double heterostructures emitting at 1.3 and 1.6 microns. Proceedings of 3rd Oxford Conference on: Microscopy of Semiconducting Materials. The Institute of Physics Conference Series Number 67, 273-278

[6] Franzosi P., Salviati G. (1985) X-ray and SEM investigation on n-type, p-type and semi-insulating GaAs. Acta Physica Hungarica 57, 251-261.

[7] Franzosi P., Salviati G. (1983) Investigation of crystal defects in GaAs by X-ray topography and SEM transmission cathodoluminescence. Materials Chemistry and Physics 9, 321-328

[8] Franzosi P., Salviati G. (1983) Room temperature transmission cathodoluminescence study of dislocations in semi-insulating GaAs single crystals. Journal of Crystal Growth 63, 419-422

[9] Holt D.B. (1974) Quantitative scanning electron microscope studies of cathodoluminescence in adamantine semiconductors. In: Quantitative Scanning Electron Microscopy, D.B. Holt, M.D. Muir, P.R. Grant, I.M. Boswarva (Eds.), Academic Press, London, pp. 335-386.

[10] Mahajan S. (1983) The sources of defects in InP/InGaAsP emitters. Proceedings of 3rd Oxford Conference on: Microscopy of Semiconducting Materials. The Institute Of Physics Conference Series Number 67 259-272

[11] Shaw D.A., Thornton P.R. (1968). Cathodoluminescence studies of laser quality GaAs. J. Mat. Sci. 3,507-518

[12] Stirland D.J., Hart D.G., Clark S., Regnault J.C., Elliot C.R. (1983) Characterization of defects in InP substrates. Journal of Crystal Growth 61,645-657

[13] Temkin H. Zipfel C.L., Keramidas V.G. (1981) High-temperature degradation of InGaAsP/InP light emitting diodes J. Appl. Phys. 52, 5377-5380.

Discussion with Reviewers

D.B. Holt: The contrast in Figure 3 is explained in terms of high, fairly high and low concentrations of Te as one proceeds outwards radially from the dislocation lines. A similar explanation in terms of a single denuded zone around a decorated dislocation, was given by Shaw and Thornton (text ref. 11) and Balk et al. (text ref. 1) who reported direct evidence for a correlation of simple dark dot contrast with Se concentration determined from emission band shift measurement. Have the authors any supporting evidence for their interpretation?
Authors: Our interpretation is based on the papers you quote.

D.B. Holt: The CL micrographs of Figures 11(a) and 12 show "grappes" (french for bunches of grapes) as they are generally known. This is a nice demonstration of the capabilities of the CL technique. These defects have been extensively studied by XRT, etching, TEM and transmission stress-birefringence infrared microscopy and recently by photoluminescence microscopy. As yet no technique has been able to identify the centres of stress responsible for grappes. Can the authors envisage any method for identifying the precipitates, voids, gas bubbles, or whatever they are, that lie at the centres of grappes?
Authors: We think that HVTEM on relatively thick samples and liquid helium spectrally resolved CL could contribute to identify the centres responsible for grappes. In a few cases after chemical etching we have found a small pit in the middle of the grappes. The pit could be consistent with the presence of gas bubbles.

D.B. Holt: In Fig. 17 could the defects in the epi-layer not have nucleated during growth rather than at the substrate interface? The last sentence supports your statement but does not prove its exclusive validity, surely?
Authors: Fig. 17 clearly shows that the defects in the epi-layer do not come from the substrate. We agree that the nucleation could occur both at the interface or later on during the growth. In our case we found that the nucleation occurs at the interface.

K. Löhnert: In an earlier CL study on GaAs:Se single crystal material (text reference 1) it has been observed, that the CL contrast of dislocations depends on the excitation density i.e. on the beam current at a given beam energy. Did you make similar observations during your studies?
Authors: On both GaAs and InP substrates considered in this study we never observed any contrast variation over a beam current range from nA to μA.

K. Löhnert: Have you tried to analyse the CL emission spectrum of the bright defects in fig. 8 or to identify their chemical composition by X-ray microanalysis?
Authors: No spectrally resolved CL measurements have been performed. X-ray point analysis showed no extraneous elements. X-ray scattering experiments performed by double crystal diffractometer confirmed the presence of microdefects.

K. Löhnert: In fig. 9 faint dark lines can be seen running perpendicular to the growth striations. Do you have an idea of what these lines are?
Authors: At present we have no explanation for these lines.

K. Löhnert: Could you please explain more closely how the four dot arrangements in fig. 11(a) arise?
Authors: A typical defect consisting of a central core from which dislocation loops are punched out in (110) directions is often present in InP substrates. Four dot arrangements, like that shown in Fig. 11a, evidence dislocation loops in the (110) directions inclined by 45° with respect to the (001) plane. Please see: D.J. Stirland et al. J. Cryst. growth 61 (1983) 645-657 and P. Franzosi, G. Salviati, R. Cocito, F. Taiariol, and C. Ghezzi, J. Crystal Growth, 69 (1984) 388-398.

A.C. Papadopoulo: What is for you the major argument for the less sensitivity to surface effects (including surface recombination) of the TCL method as compared to the ECL?
Authors: The TCL method is less sensitive to surface contamination and morphology because only the primary electrons are affected. As far as the surface recombination is concerned both TCL and ECL are affected in a similar way.

A.C. Papadopoulo: In which experimental conditions have been obtained the results corresponding to the curve of the figure 1. For the measurements did you check for the low injection conditions?
Authors: The experimental conditions used to obtain the curve of the figure 1 are: 20 kV, $1.5 \cdot 10^{-7}$ A, scanned area of about 9 mm^2, exposure time 1 minute. As you can see the measurements were performed in low injection level conditions.

A.C. Papadopoulo: Are not the growth striations related more to constitutional supercooling than to the stresses during the growth?
Authors: Our statement is simply that the stress is responsible for XRT contrast. Our study does not deal with the origin of the growth striae.